Available online at www.sciencedirect.com
ScienceDirect
International Journal of Heat and Mass Transfer 51 (2008) 3582–3594
International Journal of HEAT and MASS TRANSFER
www.elsevier.com/locate/ijhmt

# Thermal performance of a multi-block heat exchanger designed on the basis of Bejan's constructal theory

V. Arun Prasad Raja [a], Tanmay Basak [b], Sarit Kumar Das [a,*]

[a] Heat Transfer and Thermal Power Laboratory, Department of Mechanical Engineering, Indian Institute of Technology Madras, Chennai 600 036, India
[b] Department of Chemical Engineering, Indian Institute of Technology Madras, Chennai 600 036, India

Received 5 March 2007; received in revised form 24 August 2007
Available online 8 January 2008

**Abstract**

In the present work, the design and analysis of a multi-block heat exchanger has been carried out by applying the concept of constructal theory proposed by Bejan. The heat exchanger works on the principle of developing laminar flow in each block carefully designed to avoid fully developed heat transfer coefficient. The additional thermal interaction is provided by the special design allowing heat transfer in ports as well as collecting and distributing channels. Numerical simulations were carried out for different values of heat capacity rate ratios on finned and unfinned constructal heat exchangers and four cross flow heat exchangers (two finned and two unfinned). In all the heat exchangers the heat transfer area is kept the same. To validate the numerical results, experiments were conducted keeping the heat transfer area and boundary conditions same as that of the numerical simulations. The results show that the effectiveness of the constructal heat exchangers, both finned and unfinned, are higher by around 20% compared to that of the conventional cross flow heat exchangers under similar conditions. The experimental result confirms this enhancement and brings out the immense potential of this new type of heat exchanger.


*Keywords:* Heat exchangers; Constructal theory; Compact surfaces; Geometrical optimisation; Thermal entry length

## 1. Introduction

Heat exchangers play a major role in process industries, power generation, space applications, refrigeration and air-conditioning, etc. Common examples of heat exchangers are automobile radiators, air preheaters, cooling towers, condensers, evaporators, and so on. Enhancing the performance of heat exchangers is a major research effort going on throughout the world. Most of these research works are aimed at increasing the performance by providing new types of surfaces and/or fins for heat transfer. The inclination towards miniaturisation has necessitated the requirement of high heat transfer density devices in various fields. Constructal theory is a recent addition by Bejan [1–4] to the research field which is aimed at generating flow structure for maximum global performance under local constraints. The present research work is aimed at introducing a new way of improving the performance of cross flow heat exchanger by applying Bejan's constructal principle. The main motivation behind this work is the widespread application of constructal theory in engineering systems. The heat exchanger has been named as dendritic constructal heat exchanger because – just as there exists various diameter ratios between the bifurcation of tree branches, in a dendritic heat exchanger there also exists different diameter ratios between channels as the streams flow from inlet to the outlet of the heat exchanger. The available heat transfer area is distributed in such a way that the fluid enters the heat exchanger through the largest diameter channel and flows through smaller and smaller channels to reach the core section. From the core, the stream flows through larger and larger channels and comes out through

* Corresponding author. Tel.: +91 044 2257 4655; fax: +91 044 2257 4652.
*E-mail address:* skdas@iitm.ac.in (S.K. Das).

0017-9310/$ - see front matter © 2008 Elsevier Ltd. All rights reserved.
doi:10.1016/j.ijheatmasstransfer.2007.10.027

**Nomenclature**

| | |
|---|---|
| $C_p$ | heat capacity rate of fluid (J K$^{-1}$) |
| $D_0$ | elemental channel spacing (m) |
| $D_1$ | manifold wall spacing (m) as shown in Fig. 3 |
| $D_h$ | hydraulic diameter (m) |
| $h$ | heat transfer coefficient (W m$^{-2}$ K$^{-1}$) |
| $H$ | height of the manifold extension (m) |
| $k$ | thermal conductivity (W m$^{-1}$ K$^{-1}$) |
| $L$ | channel length in Fig. 3 (m) |
| $L_1$ | height of channel in Fig. 3 (m) |
| $\dot{m}$ | mass flow rate (kg/s) |
| $n$ | number of plates |
| $N$ | number of channels |
| $Nu$ | Nusselt number |
| NTU | number of transfer units of the heat exchanger |
| $P$ | pressure (Pa) |
| $Q$ | heat transfer rate in the heat exchanger (W) |
| $R$ | heat capacity rate ratio, $((\dot{m}C_p)_{min}/(\dot{m}C_p)_{max})$ |
| $t$ | plate thickness (m) cold fluid temperature (K) |
| $T$ | temperature (K) |
| $\Delta T$ | temperature difference ($T_{hi} - T_{ho}$ or $T_{co} - T_{ci}$) (K) |
| $u, v, w$ | velocities in $x$-, $y$- and $z$-directions (m s$^{-1}$) |
| $V$ | volume (m$^3$) |

*Greek symbols*

| | |
|---|---|
| $\mu$ | viscosity (kg m$^{-1}$ s$^{-1}$) |
| $\varepsilon$ | effectiveness ($=Q_{actual}/Q_{max}$) (%) |
| $\rho$ | density of fluid (kg m$^{-3}$) |
| $\nu$ | kinematic viscosity (m$^2$ s$^{-1}$) |

*Subscripts*

| | |
|---|---|
| actual | taking place in reality |
| c | cold side |
| h | hot side |
| i | inlet |
| min | minimum |
| max | maximum |
| o | outlet |

the largest channel at the outlet. This heat exchanger may be termed as constructal as the smallest channels are made first and then it is constructed by stacking these channels to form bigger structure.

Bejan [5] described the constructal route to the conceptual design of a two-stream heat exchanger with maximal heat transfer rate per unit volume. The heat exchanger flow structure described has multiple scales and the smallest scales match the thermal entrance length of the small streams that flows through the channel. Da Silva et al. [6] described the conceptual design and performance of a balanced two-stream counter flow heat exchanger. In this heat exchanger, each stream flows as a tree network through its allotted space. They stated that the two trees in counter flow are like two palms pressed against each other. They also discussed the application of dendritic heat exchangers to devices with maximal transport density. Da Silva et al. [7] reported experimentally the hydraulic and thermal behaviour of a balanced counter flow heat exchanger in which each stream flows through a tree-shaped structure covering a circular area. They concluded that the hydraulic results show a relation between the appearance of volumetric flow rate asymmetries and the bifurcation angles throughout the dendritic structure. Muzychka [8] examined the heat transfer from arrays of circular and non-circular ducts subject to finite volume and constant pressure drop constraints. It has been shown that the optimal duct dimension is independent of the array structure and hence represents an optimal construction element. Bonjour et al. [9] reported the fundamental relation between the maximization of global performance and the malleable (morphing) architecture of a flow system with global constraints. For illustration, they considered the coaxial two-stream heat exchanger with flow through a porous bed in the annular space. They showed that constraints force the design toward heat exchangers with finite axial length, where additional improvements are derived by installing high-conductivity fins across the porous bed. They concluded that when the size is small, the best is the radial pattern and when the size exceeds a certain threshold, the best configuration is the optimised branched tree of fins. Zimparov et al. [10] studied the performance of balanced two-stream parallel flow heat exchangers, in which each stream flows as a tree network. They assumed that the two trees are in parallel flow, and are arranged like two palms pressed against each other. They also compared the performance of the parallel flow configurations with the performance of counter flow configurations. They proposed the future use of dendritic heat exchangers in devices with maximal heat transport density.

From the above literature, it is clear that the application of constructal theory has been proposed for heat exchangers with many possible theoretical variations but this has not been justified on a real design of cross flow heat exchangers, which are important from the viewpoint of emerging applications. The motivation of the present work is to bridge the gap. In the current work, an attempt has been made to conceptualize and design a heat exchanger containing multiple constructs based on Bejan's constructal theory. An extensive computational analysis of a constructal heat exchanger has been carried out to evaluate its performance. Finally, experiments with constructal heat exchanger have been carried out to validate the computational predictions. The designed constructal heat exchanger

has also been compared with equivalent cross flow heat exchanger with respect to thermal and hydraulic performance both computationally and experimentally.

## 2. Constructal heat exchanger: design

The design is carried out based on Bejan's constructal principle. For a finite size system to persist (live) in time it must evolve in such a way that it provides easier access to its currents. Constructal heat exchanger flow structures are tree-shaped with multiple scales that are arranged hierarchically and their performance is expected to be much superior to the existing heat exchangers.

The key features of the constructal heat exchangers are as follows:

1. Tree-shaped collecting and distributing channels.
2. Elemental flow operates in the thermal entrance length.
3. Flow arrangement: counter flow–cross flow–counter flow.
4. Cross flow arrangement at the elemental (core) channels.
5. Counter flow arrangement in the manifolds, distributing and collecting channels.
6. Dichotomy (pairing or bifurcation) used here is an optimisation result, not an assumption.
7. Non-uniform scales.
8. Laminar flow.

The preliminary design of dendritic constructal heat exchanger is shown in Fig. 1a. This design is arrived after number of numerical simulations to find the optimal structure. Fluid mechanic optimisation for the design of the constructal heat exchanger was carried out using commercial software Fluent. The optimised design was proposed by the simulations for different combination of channel $D_h$ and flow rates.

The core section of a construct of the constructal heat exchanger may be with and without fins; the finned core is shown as cut section in Fig. 1b. Metallic mesh is provided in the inlet manifolds to avoid the backflow in the manifolds and core section which was observed in the numerical solution of the preliminary design of constructal heat exchanger. The special features in the design are the manifolds which transfer heat to the adjacent counter flow manifold of the neighbouring construct as proposed by Bejan [5] and the collecting and distributing channels effecting similar counter flow heat transfer designed judiciously here as shown in Fig. 2. It must be mentioned here that the present design deviates from Bejan [5] in practical considerations since the proposed block type collecting and distributing channel brings wastage of material due to machining and unequal channel spacing suggested by him to counter flow maldistribution is not practical from manufacturing view point. The flow maldistribution is reduced here by successive simulations to adjust port to channel area ratio. In this design process the various dimensions were arrived at using the constructal theory as follows.

To achieve maximum heat transfer per unit volume, every infinitesimal packet of fluid must be used for the purpose of transferring heat. This is possible only if the channel length matches the thermal entry length of the small stream that flows through it. The constructal heat exchanger has been designed with uniform elemental channel spacing and straight $D_1$ channels as shown in Fig. 3.

Practically, it is not possible to match all the elemental channel length with the thermal entry length due to flow maldistribution and manufacturing difficulties. Hence, this feature is avoided in the present design and the channel length is designed to be smaller than the smallest thermal entry length i.e. the flow will be thermally developing. However, the overall heat transfer coefficient is higher than that of the fully developed flow condition. The most important dimension is the elemental channel dimensions as most of the heat transfer takes place in these elemental channels.

The following equation is used for finding the thermal entry length for rectangular channels:

$$\left(\frac{L_T/D_h}{Re_{D_h}Pr}\right)^{1/2} \cong 0.2, \tag{1}$$

where $Re_{D_h} = U_0 D_h/\nu$, with $\nu$ as the kinematic viscosity of the fluid, and $D_h$ as the hydraulic diameter, $D_h = 2D_0$. Selecting the elemental flow length such that $L < L_T$, we find from Eq. (1) that

$$\frac{L}{D_0} \leqslant 0.16\frac{U_0 D_0}{\nu}Pr > 1. \tag{2}$$

If $D_0$ is the smallest channel dimension, then $L$ may be obtained from Eq. (2) when $U_0$ is known.

The elemental velocity, $U_0$ may be estimated if the volume and macroscopic streams of the entire heat exchanges are specified. Let $V$ and $m_h$ be the total volume and the mass flow rate of the hot streams that must be distributed throughout $V$. According to the constructal method, the volume $V$ is filled by interconnected elemental volumes. The order of magnitude of the cross-sectional area of $V$ is $V^{2/3}$. As given in Bejan [5], the stream $m_h$ perfuses with the velocity $U_0$ through the area $V^{2/3}$, therefore, from mass conservation

$$U_0 \approx m_h/(\rho V^{2/3}). \tag{3}$$

Due to computational and experimental limitations, the present study is limited to a heat exchanger with four constructs which can be extended to multiple constructs for higher heat duties.

## 3. Numerical study

The numerical analysis of the above heat exchanger has been carried out to access its performance. The details of the geometrical configurations are shown in Table 1. The computational domain is limited to the geometry of the heat exchanger. It is not extended beyond the inlet and outlet port since for strong unidirectional forced convection this was not found to be necessary. It should be noted here that in order to bring out the relative enhancement of per-

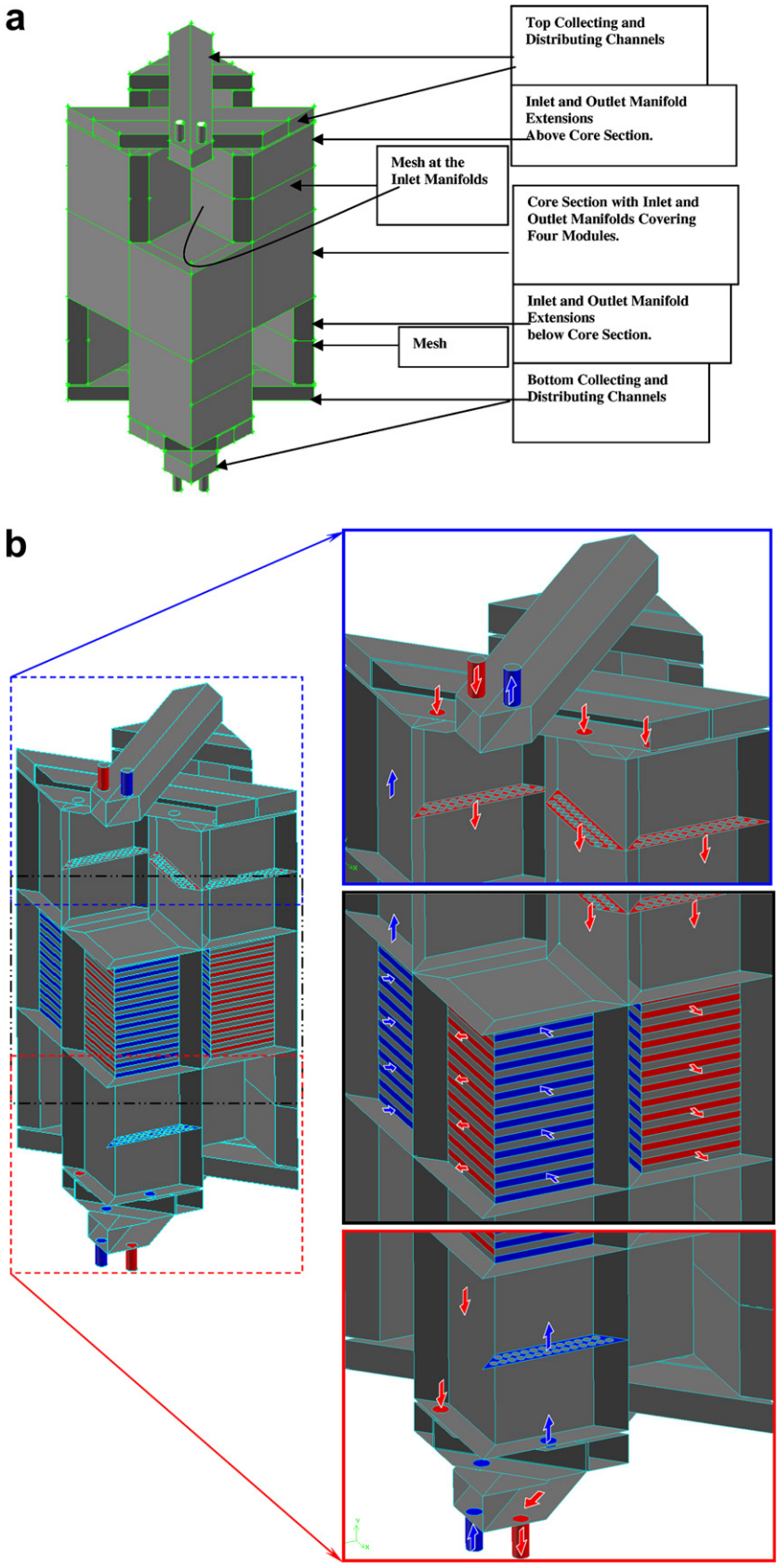


Fig. 1. Constructal heat exchanger: (a) solid model; (b) detailed isometric view of dendritic constructal heat exchanger with manifold extensions.

formance two cross flow heat exchangers with identical heat transfer area are also simulated. These two heat exchangers are chosen to be of 33 channels (33 CH HX) and 9 channels (9 CH HX). This is chosen to differentiate

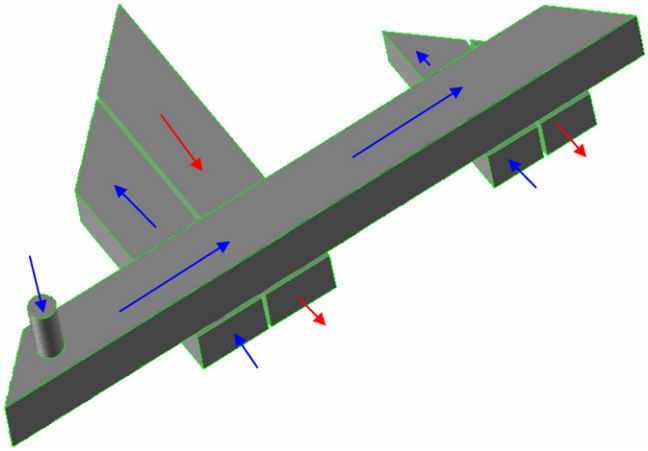

Fig. 2. Collecting and distributing channels.

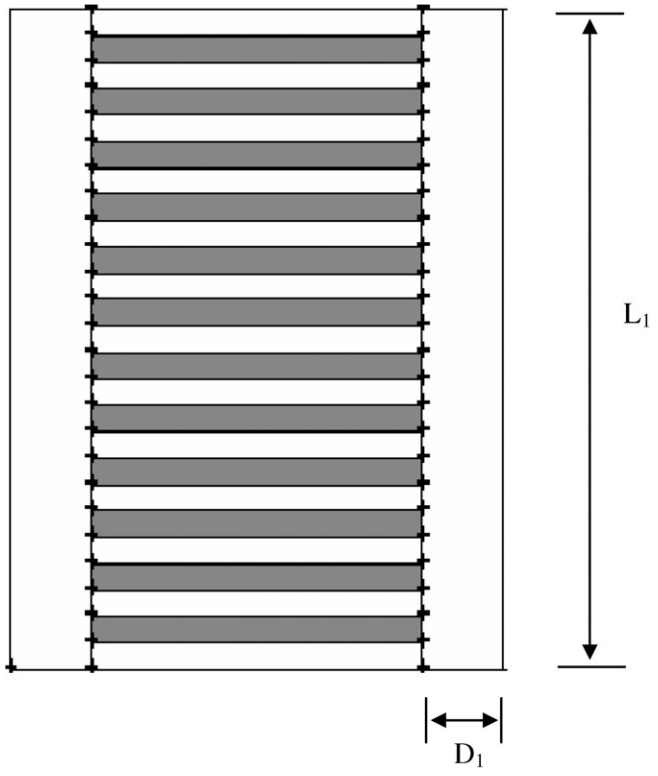


Fig. 3. Straight $D_1$ channels and uniform channel spacing in a block of constructal heat exchanger.

between the effect of developing flow and port/collecting–distributing channel heat transfer. While the constructal heat exchanger has got both the effects, the 33 CH HX has got only the developing flow effect and the 9 CH HX has very little amount of either effect. The two cross flow heat exchangers are shown in Figs. 4a and 4b.

### 3.1. Governing equations

The governing equations for mass, momentum and energy are as follows:

$$\frac{\partial u}{\partial x}+\frac{\partial v}{\partial y}+\frac{\partial w}{\partial z}=0, \tag{4}$$

$$\rho\left(u\frac{\partial u}{\partial x}+v\frac{\partial u}{\partial y}+w\frac{\partial u}{\partial z}\right)=-\frac{\partial P}{\partial x}+\mu\left(\frac{\partial^2 u}{\partial x^2}+\frac{\partial^2 u}{\partial y^2}+\frac{\partial^2 u}{\partial z^2}\right), \tag{5}$$

$$\rho\left(u\frac{\partial v}{\partial x}+v\frac{\partial v}{\partial y}+w\frac{\partial v}{\partial z}\right)=-\frac{\partial P}{\partial y}+\mu\left(\frac{\partial^2 v}{\partial x^2}+\frac{\partial^2 v}{\partial y^2}+\frac{\partial^2 v}{\partial z^2}\right), \tag{6}$$

$$\rho\left(u\frac{\partial w}{\partial x}+v\frac{\partial w}{\partial y}+w\frac{\partial w}{\partial z}\right)=-\frac{\partial P}{\partial z}+\mu\left(\frac{\partial^2 w}{\partial x^2}+\frac{\partial^2 w}{\partial y^2}+\frac{\partial^2 w}{\partial z^2}\right), \tag{7}$$

$$\rho C_p\left(u\frac{\partial T}{\partial x}+v\frac{\partial T}{\partial y}+w\frac{\partial T}{\partial z}\right)=k\left(\frac{\partial^2 T}{\partial x^2}+\frac{\partial^2 T}{\partial y^2}+\frac{\partial^2 T}{\partial z^2}\right). \tag{8}$$

### 3.2. Boundary conditions

Mass flow rate is specified at the inlets of the hot and the cold stream. The pressure is specified for hot and cold stream at the outlet. The hot stream inlet temperature ($T_{hi}$) is 330 K and the cold stream inlet temperature ($t_{ci}$) is 304 K. The outer walls of the heat exchangers are insulated and hence an adiabatic condition is applied on them.

Boundary condition are as follows:

At inlet: velocity, $V=$ constant,
$T_{ci}=304$ K,
$T_{hi}=330$ K for unfinned HX,
$T_{hi}=345$ K for finned HX.
At outlet: static pressure, $P=0$.

### 3.3. Simulation procedure

The following assumptions are made for the simulation:

1. Fluid flow is steady and incompressible.
2. Thermophysical properties are kept constant at mean value.

The numerical details of the simulation are as follows:

1. Pressure–velocity coupling is done by SIMPLE algorithm.
2. For convective kinematics second order upwind scheme is used.
3. Convergence criterion for momentum is $10^{-6}$ and for energy it is $10^{-9}$.

Numerical simulations were carried out using the CFD software FLUENT 6.2. The geometries and grids are created using GAMBIT.

### 3.4. Grid independence

Grid independence tests were carried out and the numbers of grid points necessary for obtaining the grid independent results arrived. A grid independence test is shown in Fig. 4c for channel Nusselt number. The typical grids required for the simulation are shown in Table 2.

Table 1
Details of the heat exchangers used for simulations

| Heat exchanger type | Single core channel volume ($mm^3$) | Total height (m) | Number of channels in each block | Number of blocks | Number of core heat transfer plates | Number of plain fins provided at the core channels | Heat transfer area in cross flow, $m^2 \times 10^{-2}$ | Heat transfer area in counter flow, $m^2 \times 10^{-2}$ | [a]Compactness |
|---|---|---|---|---|---|---|---|---|---|
| *Unfinned heat exchangers* | | | | | | | | | |
| 9 CH HX | $100 \times 100 \times 2$ | 0.180 | 9 | 1 | 8 | – | 8 | – | 1000 |
| 33 CH HX | $50 \times 50 \times 2$ | 0.220 | 33 | 1 | 32 | – | 8 | – | 1000 |
| Constructal HX | $25 \times 25 \times 2$ | 0.345 | 25 | 4 | 96 | – | 6 | 2 | 409 |
| *Finned heat exchangers* | | | | | | | | | |
| 7 CH HX | $117 \times 117 \times 2$ | 0.180 | 7 | 1 | 6 | 12 | 8.52 | – | 1073 |
| 25 CH HX | $57.5 \times 57.5 \times 2$ | 0.220 | 25 | 1 | 24 | 52 | 8.52 | – | 1037 |
| Constructal HX | $25 \times 25 \times 2$ | 0.345 | 25 | 4 | 96 | 104 | 6.52 | 2 | 435 |

[a] Compactness $= A_h/V_h$ or $A_c/V_c$ for plate, plate-fin heat exchangers.

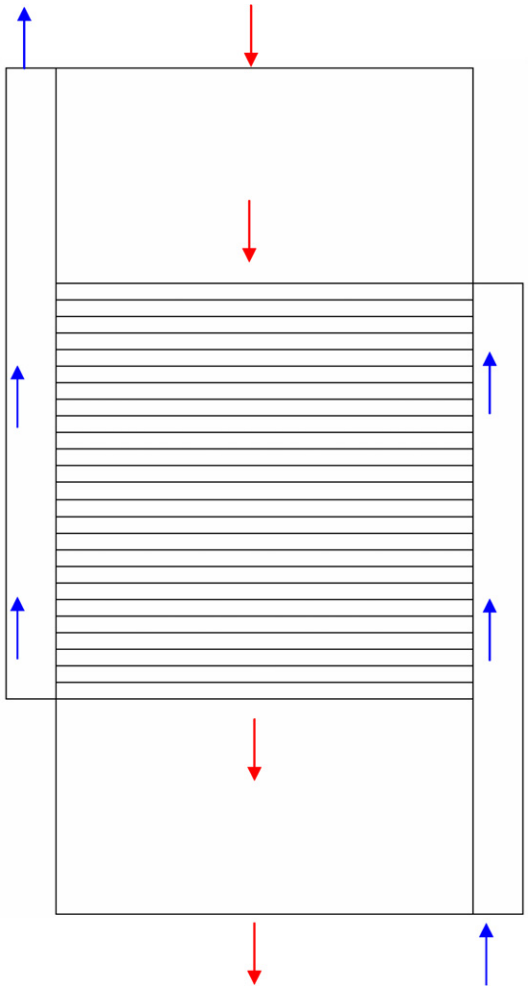

Fig. 4a. The cut sectional view of 33-channel heat exchanger.

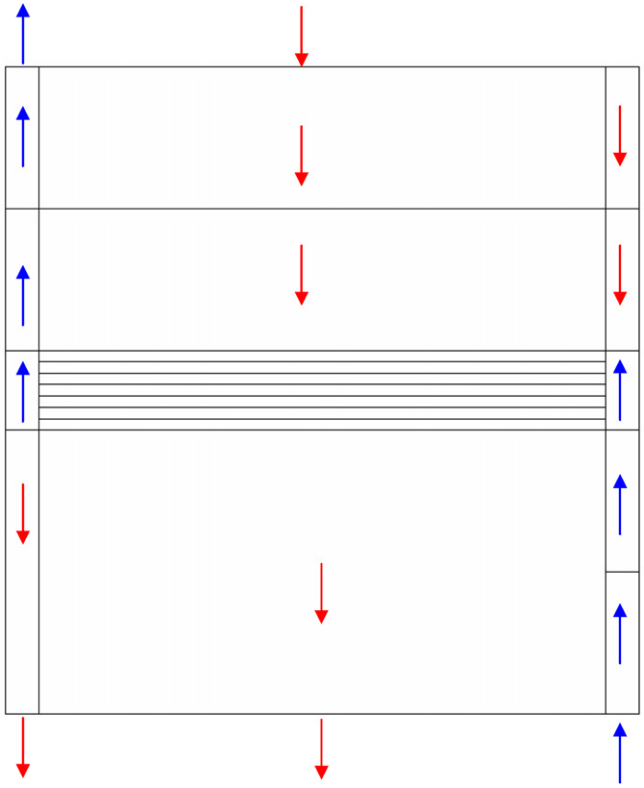

Fig. 4b. The cut sectional view of 7-channel heat exchanger.

## 4. Experimental study

The fabricated constructal heat exchanger is as shown in Fig. 5a. The material of construction is copper with plate thickness of 0.3 mm. The details of the dimension are given in Table 1. The heat exchangers are made by brazing using lead–silver (60–40%) alloy. In the manufacturing process, initially, copper plates of dimension $(L + 4\,\text{mm}) \times (W + 4\,\text{mm})$ are cut. The additional 4 mm added to the length ($L$) and width ($W$) of the plate dimension is to provide the side walls of the channels with 2 mm height. The additional 4 mm along the length direction are bent downwards with 2 mm at the channel entrance and 2 mm at the channel exit, while, the additional 4 mm along the width direction are bent upwards with 2 mm at the channel left side and 2 mm at the channel right side. After the plates

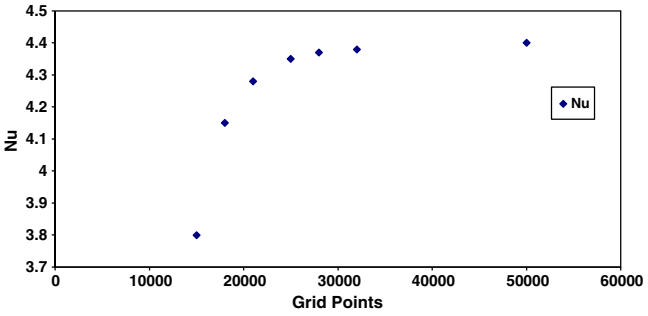


Fig. 4c. Graphical representation of a grid independence test.

Table 2
Grid points

| Heat exchanger type | Total grid points |
|---|---|
| *Unfinned heat exchangers* | |
| Constructal HX | 39,65,632 |
| 33 CH HX | 5,72,896 |
| 9 CH HX | 5,23,838 |
| *Finned heat exchangers* | |
| Constructal HX | 42,59,726 |
| 25 CH HX | 5,56,174 |
| 7 CH HX | 4,77,890 |

are cut to the above dimensions, they are placed one above the other and brazed. The resulting structure forms the core section of the heat exchangers. Then the manifold plates of dimension $L_1$ ($=D_0N + 0.3tn + 50$, mm) are cut. The additional 50 mm forms the wall portion of the manifold extension. This manifold extension is provided mainly to enable the provision of mesh at a vertical distance of 25 mm from the core section. To arrest backflow, a mesh is provided only in extended portion of the inlet manifolds. The gap between the manifold wall and the core section is 6 mm. The one side opening of manifold extension portion above the core section is then closed using ($L \times H$) plates. It is to be noted that nipples of diameter 4 mm and height 5 mm are brazed at the top of extended manifolds. The resulting structure forms the complete 33 channel and 9 channel heat exchangers each with two inlets and two outlets. In case of the constructal heat exchanger, there are four blocks each with two inlets and two outlets resulting in 8 inlets (4 cold inlets and 4 hot inlets) and 8 outlets (4 hot outlets and 4 cold outlets). All the cold inlets and cold outlets have been connected in such a way that it results in a single cold inlet and a single cold outlet. The collecting and distributing channels are placed diagonally above the core section to facilitate the collecting and distributing of fluid from and to the four blocks. Two trapezoidal channel structures are placed immediately above the nipples. Each of these trapezoids are divided into two smaller trapezoidal channels, one for cold fluid and one for hot fluid, along its longest length. Out of four trapezoids, one of these trapezoids distributes the hot fluid to three blocks while the other trapezoid distributes hot fluid to one block. Out of the remaining two trapezoidal channels, one collects the cold fluid from three blocks while the other collects cold fluid from one block. To the top surface of the four trapezoids nipples are brazed resulting in two hot inlets and two hot outlets. Above these nipples, a bigger trapezoidal channel is brazed which has one inlet and one outlet as shown in Fig. 5b. To facilitate hose connection between two nipples, one for hot inlet and one for cold outlet, are brazed at its top surface. The difficulty in commercial manufacturing of a multi-block heat exchanger lies in brazing the small $D_h$ channel walls, placing the metallic mesh in the inlet manifolds of hot and cold fluids, making it leak proof for a design involving multiple bends and joints.

Experiments were conducted under steady state to test the performance of the three heat exchangers. The schematic view of the experimental setup is as shown in Fig. 6. Pumps were used for circulating the distilled water on both the hot and cold water sides of the heat exchangers. The flow rates were measured using orifice meters and controlled using gate

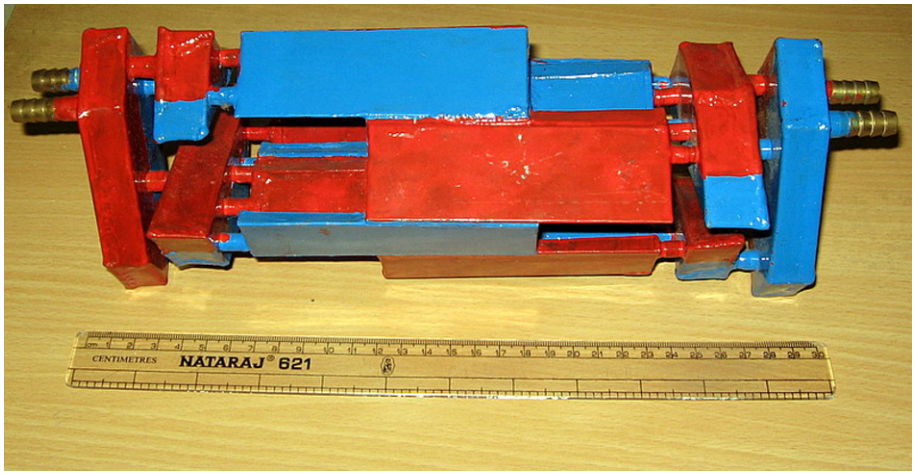


Fig. 5a. The dendritic constructal heat exchanger with small-scale cross flows and larger-scale counter flows.

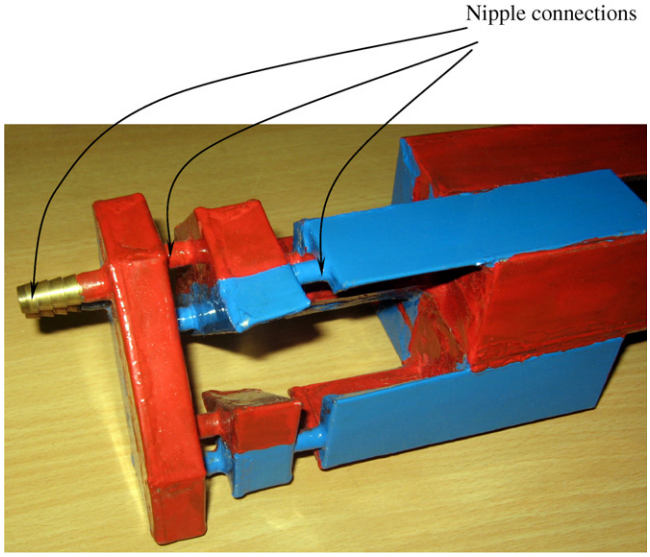


Fig. 5b. Nipple connections in the dendritic constructal heat exchanger.

valves. The temperatures at the inlets and outlets were measured using 3-wire RTDs which were connected to the data logger. U-tube manometers were used for pressure measurement. Carbon tetrachloride was used as manometric fluid. Experimentally, pressure drop was calculated by measuring the difference in the heights ($h$) between the two limbs of carbon tetrachloride filled U-tube manometer.

The heat exchangers were perfectly insulated using foam insulation to prevent heat loss into the surroundings. The experiments were conducted at different mass flow rates. It is ensured that the energy balance is within 3% deficit. The uncertainty in the flow rate is estimated to be maximum 5.23%, temperature within ±0.1 °C, Reynolds number 1.04% and pressure 2%.

## 5. Results and discussion

### 5.1. Numerical predictions

A typical velocity contour at the core section of the heat exchanger on cold and hot side are shown in Fig. 7a and b, respectively. It can be observed that the velocity is not the same in all the channels. The velocity is higher in the channels closer to the manifold outlet. This is due to lower resistance near the manifold exit and the fluid's tendency to travel through the lower resistance path. Also, temperature contour on cold and hot side are shown in Fig. 8a and b. Due to flow maldistribution, the fluids undergo different temperature changes i.e. higher temperature for channels with lower flow rates and vice versa.

It may be mentioned here that it is not possible to define NTU in constructal heat exchangers due to the fact that heat transfer takes place not only in the core channels but also in the ports and collecting/distributing channels. Hence the results are obtained here to compare between heat exchangers with identical inlet temperatures and flow rates.

In Fig. 9, it is observed that the effectiveness decreases nonlinearly with the increase in mass flow rate. The effectiveness is found to vary from 74.12% to 47.44% for constructal heat exchanger, while it is 54.41–36.21% for 33 channel heat exchanger and 50.23–34.14% for 9 channel heat exchanger. The maximum effectiveness of constructal heat exchanger is found to be 19.71% higher than that of the 33 channel heat exchanger and 23.89% higher than that of 9 channel cross flow heat exchanger. This increase in effectiveness is due to (i) the tree-shaped counter flow arrangement in the manifolds, distributing and collecting channels and (ii) core channels operating within the thermal entrance length. The nonlinear behaviour is observed

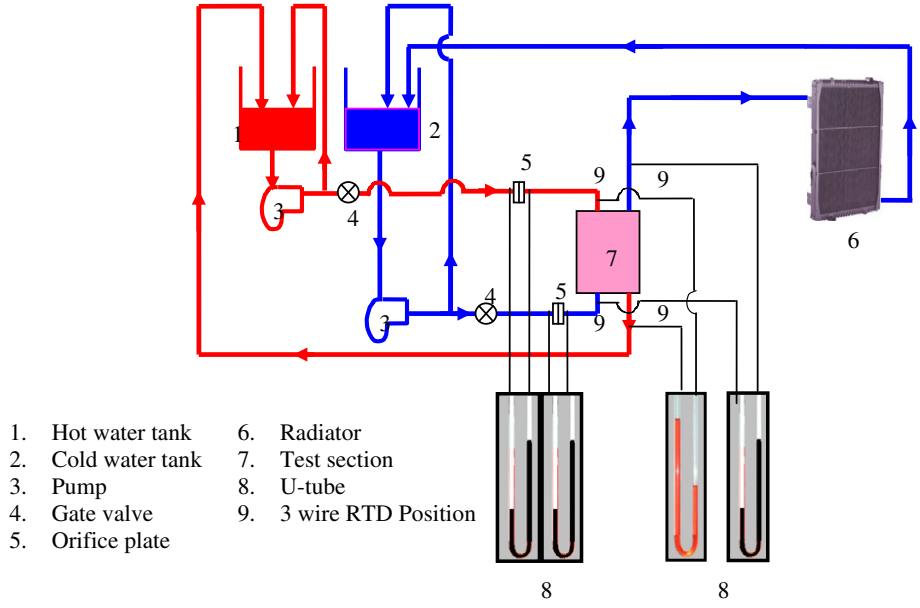


Fig. 6. Schematic diagram of the experimental test facility.

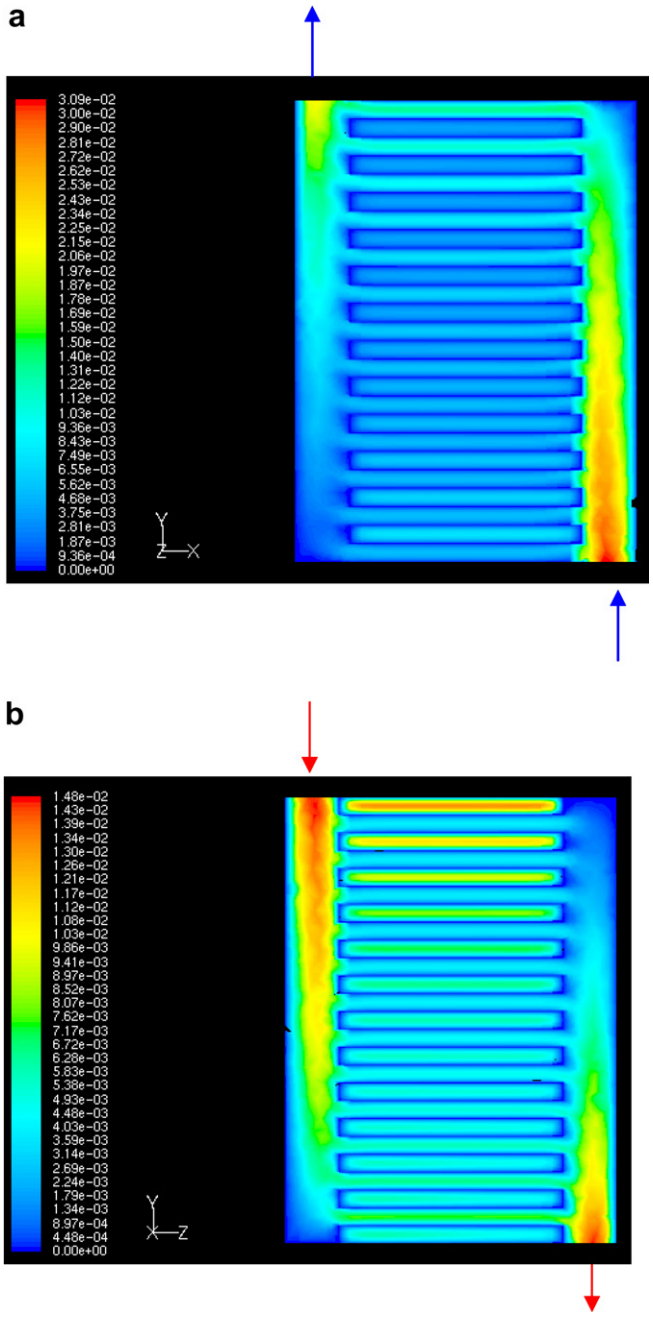


Fig. 7. Velocity contours at the core section: (a) cold fluid; (b) hot fluid.

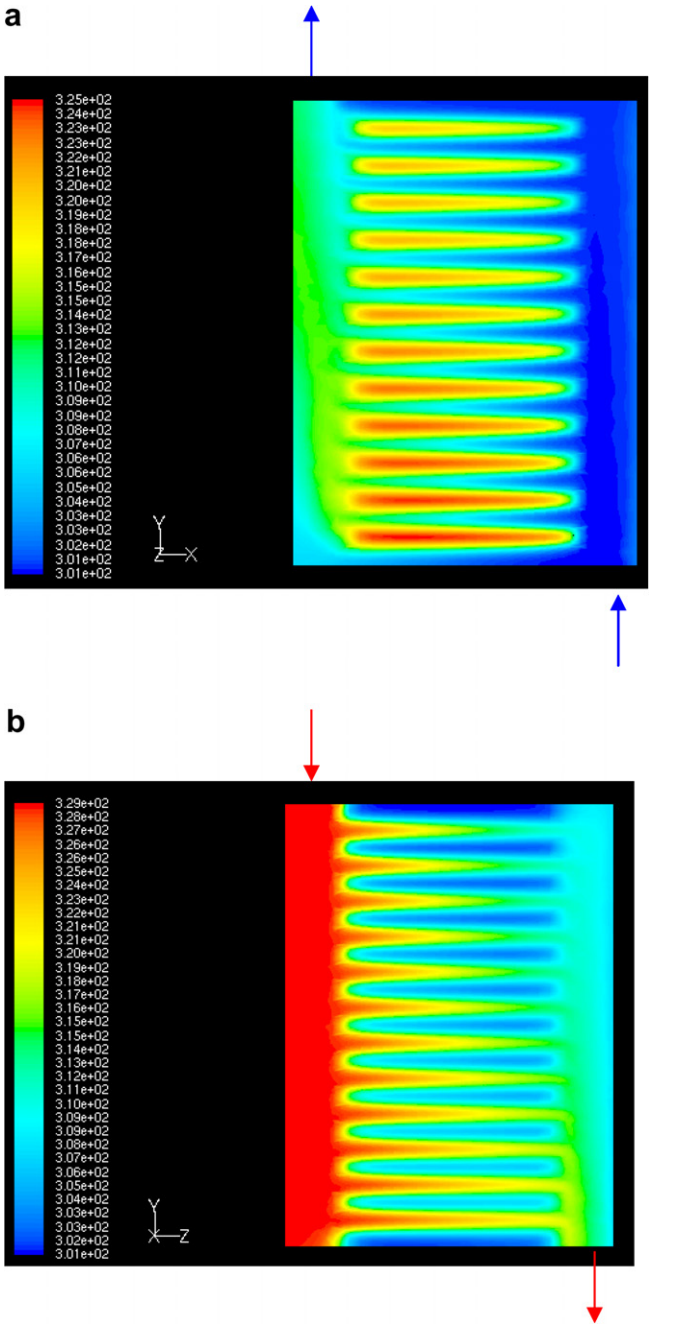


Fig. 8. Temperature contours at the core section: (a) cold fluid; (b) hot fluid.

due to two reasons, firstly the nonlinear variation of heat transfer coefficient with flow mean velocity ($\propto u_m^{1/3}$) for thermally developing laminar internal flow and secondly wider range of flow rates considered for analysis, for $R = 1$ (heat capacity rate ratio $R = C_{\min}/C_{\max}$). The maximum effectiveness of 33 CH HX is found to be higher than the 9 CH HX by 8.32%. This is due to the higher heat transfer coefficient due to entry length effect in the shorter 33 CH HX.

In Fig. 10, for $R = 0.6$, the variation of effectiveness with mass flow rate is plotted. The maximum effectiveness of constructal heat exchanger is found to be 16.74% higher than that of the 33 channel heat exchanger and 20.35% higher than that of 9 channel cross flow heat exchanger. The behaviour is similar to that observed for $R = 1$ due to the reasons mentioned already. The values of effectiveness are tabulated in Table 3.

For cold side mass flow rate of 0.008 kg/s, between $R = 1$ and 0.8, it is observed that for constructal heat exchanger, the effectiveness is around 50% and 65%, respectively. It is also observed that for cold side mass flow rate of 0.012 kg/s, with $R = 0.8$ and 0.6, for constructal heat exchanger, the effectiveness is around 54% and 70%,

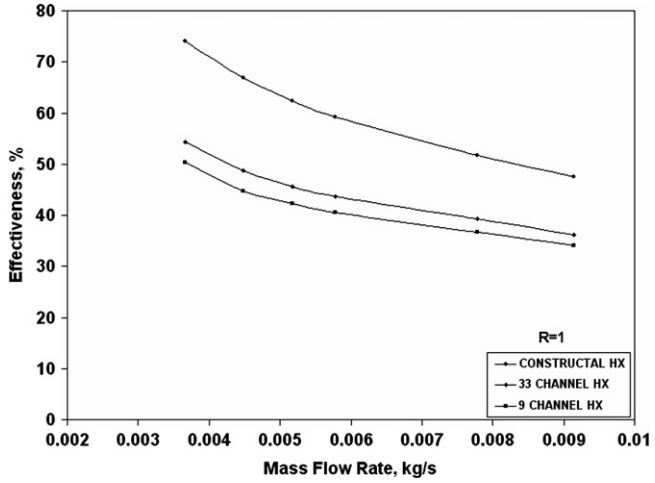


Fig. 9. Variation of effectiveness with mass flow rate for $R = 1$.

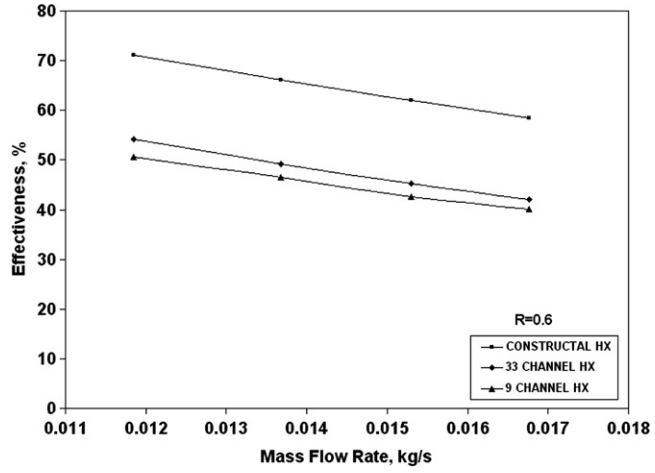


Fig. 10. Variation of effectiveness with mass flow rate for $R = 0.6$.

respectively. As $R$ value is decreased, the effectiveness is found to increase substantially. This is due to the higher temperature change undergone by the fluid with minimum heat capacity rate ($C_{min}$) at smaller $R$ values. The higher temperature change of the fluid with $C_{min}$ is due to the higher flow rate of the fluid with maximum heat capacity rate ($C_{max}$).

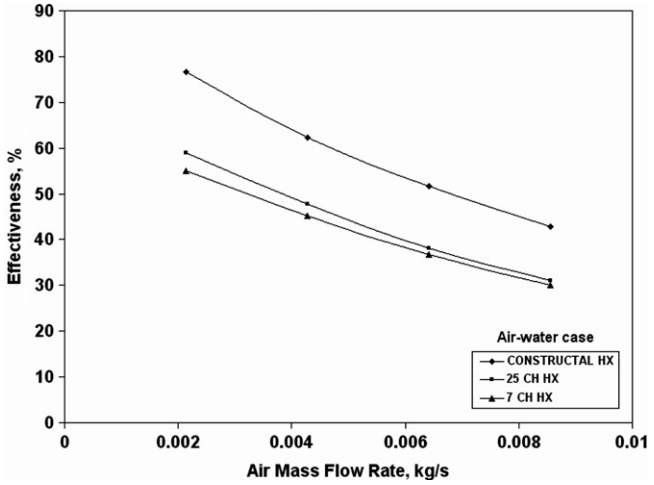


Fig. 11. Variation of effectiveness with air mass flow rate for $R = 14.7$.

In Fig. 11, the variation of effectiveness with mass flow rate, for air side finned heat exchangers are plotted. In case of finned heat exchanger, due to increase of surface area of the fins the equivalent cross flow heat exchangers are of 7 and 25 channels only (7 CH HX and 25 CH HX). It is observed that the effectiveness of the constructal heat exchanger is higher than the 25 CH HX and 7 CH HX. This increase is due to the reasons mentioned before. It is interesting to observe the high values of effectiveness in this case which is not achievable by identical cross flow heat exchangers due to attainment of asymptotic limit.

In Fig. 12, the variation of pressure drop with mass flow rate is presented, for $R = 1$. The dotted line represents the hot side while the continuous line represents the cold side. In all the three heat exchangers, it is observed that the hot side pressure drop is lower than the cold side pressure drop. This is due to the lower viscosity of the hot fluid. The pressure drop of constructal heat exchanger is higher due to (i) channels operating in the entrance region, (ii) higher number of 90° turns (iii) higher number of channels giving flow maldistribution and (iv) smaller channel hydraulic diameter. The maximum pressure drop on the cold side is found to be 11066.9 Pa while that on the hot side to be 10462.6 Pa for constructal heat exchanger; while it is 8106 Pa and 7702.33 Pa for 33 channel heat exchanger; 7126.23 Pa and

Table 3
Effectiveness for different $R$ values

| Cold side mass flow rate, $\times 10^{-3}$ kg/s (for $R = 1$) | Effectiveness for $R = 1$ | | | Cold side mass flow rate, $\times 10^{-3}$ kg/s (for $R = 0.8$) | Effectiveness for $R = 0.8$ | | | Cold side mass flow rate, $\times 10^{-3}$ kg/s (for $R = 0.6$) | Effectiveness for $R = 0.6$ | | |
|---|---|---|---|---|---|---|---|---|---|---|---|
| | Constructal HX | 33 CH HX | 9 CH HX | | Constructal HX | 33 CH Hx | 9 CH HX | | Constructal HX | 33 CH HX | 9 CH HX |
| 3.657 | 74.12 | 54.41 | 50.23 | 7.226 | 68.65 | 48.62 | 45.23 | 11.85 | 71.01 | 54.27 | 50.56 |
| 4.479 | 66.93 | 48.76 | 44.65 | 8.852 | 63.52 | 44.68 | 42.05 | 13.68 | 66.02 | 49.13 | 46.45 |
| 5.171 | 62.29 | 45.63 | 42.28 | 10.221 | 59.64 | 41.46 | 39.47 | 15.3 | 62.06 | 45.21 | 42.64 |
| 5.782 | 59.22 | 43.69 | 40.56 | 11.433 | 56.23 | 39.41 | 37.46 | 16.76 | 58.48 | 42.42 | 40.11 |
| 7.787 | 51.62 | 39.22 | 36.66 | 12.518 | 52.96 | 37.28 | 35.42 | – | – | – | – |
| 9.142 | 47.44 | 36.21 | 34.14 | – | – | – | – | – | – | – | – |

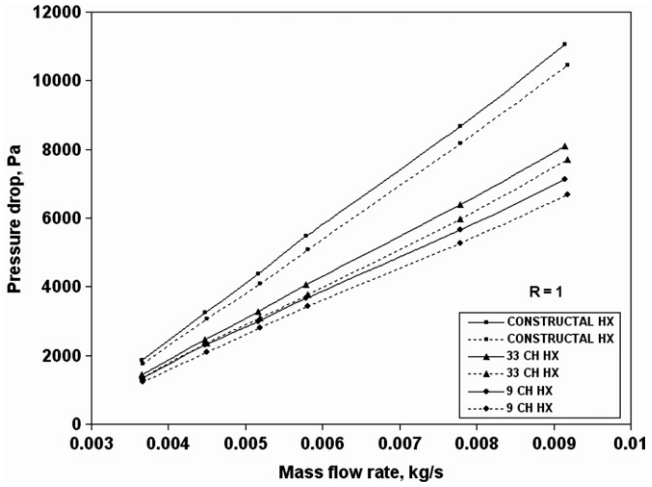


Fig. 12. Variation of pressure drop with mass flow rate for $R = 1$.

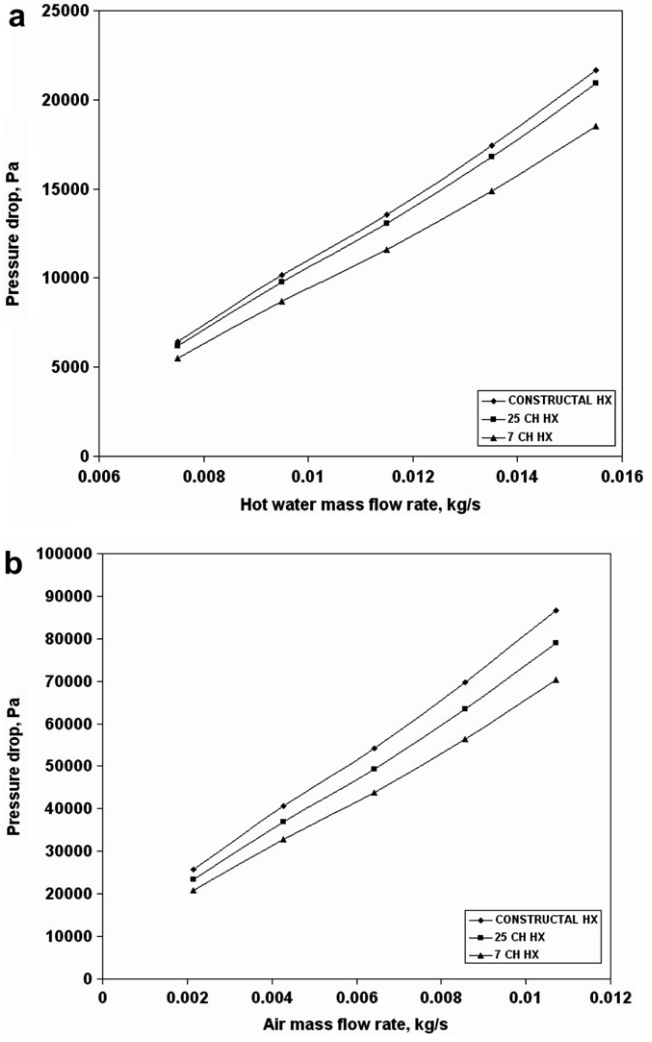


Fig. 13. Variation of pressure drop with mass flow rate for finned heat exchangers: (a) hot water side; (b) cold air side.

6672.3 Pa for 9 channel heat exchanger. The maximum pressure drop for the constructal heat exchanger is found to be higher than that of the 33 channel heat exchanger by 36.5% and 35.84% on the cold side and hot side, respectively. While compared to 9 channel heat exchanger the maximum pressure drop of constructal heat exchanger is higher by 55.29% and 56.8% on the cold side and hot side, respectively. The minimum pressure drop on the cold side is found to be 1861.2 Pa and that on the hot side to be 1749.32 Pa for constructal heat exchanger; while it is 1431.38 Pa and 1354.65 Pa for 33 channel heat exchanger; 1345.12 Pa and 1220 Pa for 9 channel heat exchanger. The minimum pressure drop for the constructal heat exchanger is found to be higher than that of the 33 channel heat exchanger by 30% and 29% on the cold side and hot side, respectively. While compared to 9 channel heat exchanger the minimum pressure drop of constructal heat exchanger is higher by 38.36% and 43.4% on the cold side and hot side, respectively. Between 33 channel and 9 channel heat exchangers, it is observed that the maximum pressure drop of 33 channel heat exchanger is 13.75% and 15.43% higher than that of 9 channel heat exchanger on the cold side and hot side, respectively.

In Fig. 13a and b, the variation of pressure drop with mass flow rate for finned heat exchangers are plotted for water side and air side, respectively. It is observed that the pressure drop on the air side is around four times higher than on the water side. This is due to the high velocity on the air side compared to that on the water side. The pressure drop of constructal heat exchanger on the hot water side is observed to be around 10% and 14% higher than the 25 CH HX and 7 CH HX. This difference is due to the reasons already discussed.

### 5.2. Experimental validation

The experimental results and numerical results are compared for all the three heat exchangers. It is found that the experimental results are in good agreement with the numer-

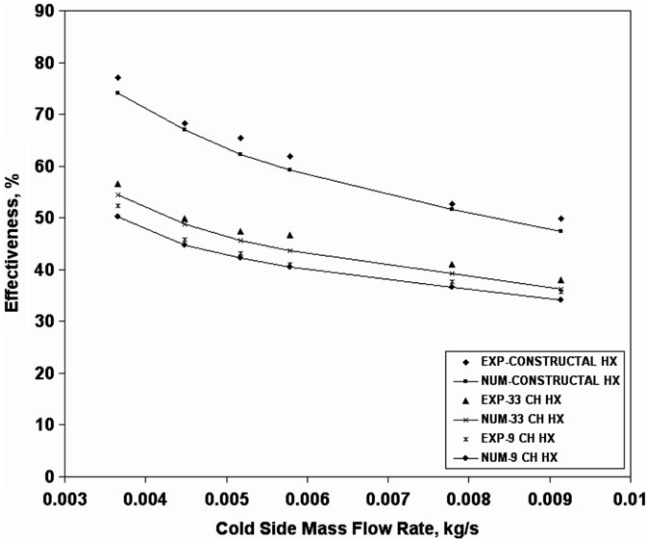


Fig. 14. Variation of effectiveness with mass flow rate for $R = 1$.

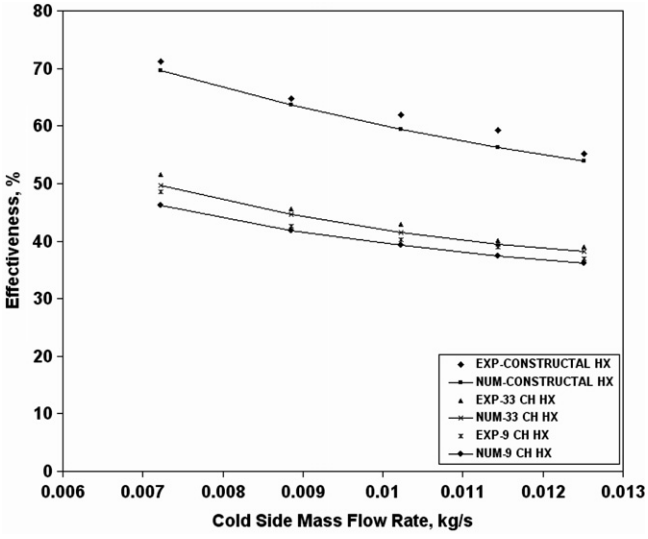


Fig. 15. Variation of effectiveness with mass flow rate for $R = 0.8$.

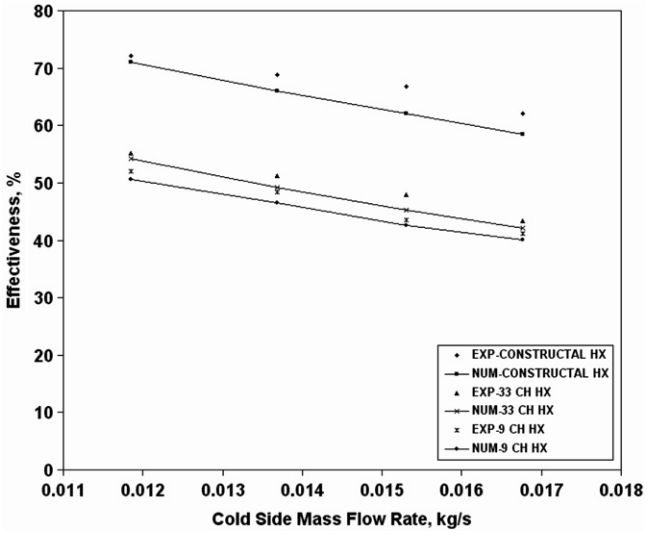


Fig. 16. Variation of effectiveness with mass flow rate for $R = 0.6$.

ical predictions. The deviation of the experimental values from the numerical predictions is found to be within ±6%. The enhancement in effectiveness is much larger than the deviation.

In Figs. 14–16, the comparison of effectiveness with flow rate between experimental and numerical results are plotted for $R = 1$, 0.8, and 0.6, respectively. The deviation of experimental values from the numerical predictions is found to be acceptable. This deviation may be due to the error in flow rate measurement and single point temperature measurement in experiments.

In Figs. 17 and 18, the pressure drop variation is plotted with mass flow rate, for $R = 1$. It is observed that the experimental values are in good agreement with the numerical results. The deviation of experimental values from the numerical predictions is found to be within ±8%.

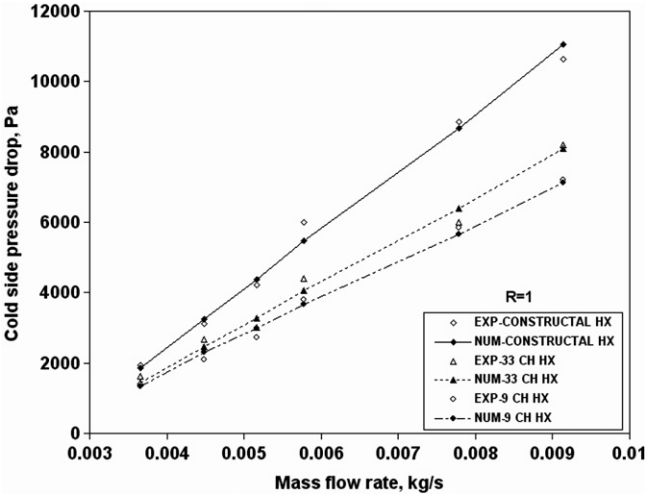


Fig. 17. Variation of pressure drop with mass flow rate (cold fluid) for $R = 1.0$.

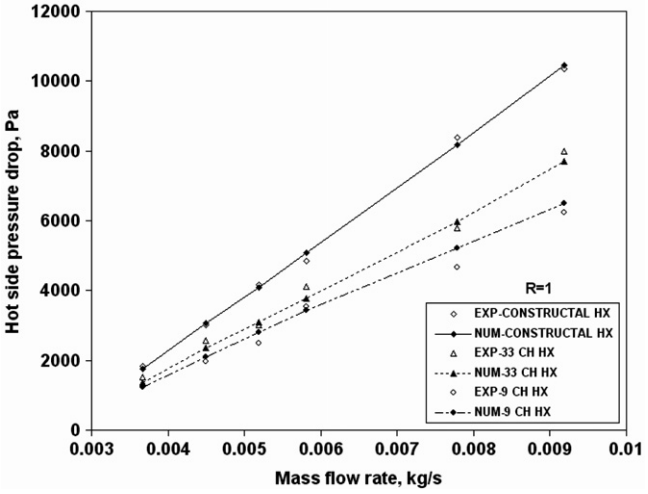


Fig. 18. Variation of pressure drop with mass flow rate (hot fluid) for $R = 1.0$.

## 6. Conclusions

In unfinned dendritic constructal heat exchanger,

(i) For $R = 1.0$ the maximum effectiveness of cross flow heat exchangers is 56.5% whereas it is 77% for constructal heat exchanger.
(ii) For $R = 0.8$ the maximum effectiveness of cross flow heat exchangers is 51.6% whereas it is 71% for constructal heat exchanger.
(iii) For $R = 0.6$, the maximum effectiveness of cross flow heat exchangers is 55.19% whereas it is 72% for constructal heat exchanger.

In air side finned dendritic constructal heat exchanger:

(i) For $R = 14$, the effectiveness of cross flow heat exchangers is 59%, whereas it is 76.55% for constructal heat exchanger.

Constructal heat exchangers can achieve the performance (effectiveness) which cannot be achieved by conventional cross flow heat exchangers under the same operating conditions. Pressure drop of constructal heat exchangers is 20–32% higher than the cross flow heat exchangers. The pressure drop is higher due to the complex tree-shaped flow structure. However, the pressure drop is still at a low value in absolute sense. The maximum pressure drop is less than 25 kPa for unfinned constructal heat exchangers and is less than 90 kPa for finned constructal heat exchanger.

The benefit in effectiveness in constructal heat exchangers is more than the loss due to higher pressure drop. In fact, to get the same effectiveness as that of the cross flow heat exchangers, much lesser heat transfer area will be sufficient for constructal heat exchanger, thereby reducing the cost, space occupied and pressure drop. Hence, it is concluded that the constructal heat exchanger can, in fact, replace the conventional cross flow heat exchangers in many applications in the near future.

## References

[1] A. Bejan, Constructal-theory network of conducting paths for cooling a heat generating volume, Int. J. Heat Mass Transfer 40 (4) (1997) 799–810.

[2] A. Bejan, Constructal theory: from thermodynamic and geometric optimization to predicting shape in nature, Energy Convers. Manage. 39 (16–18) (1998) 1705–1718.

[3] A. Bejan, How nature takes shape: extensions of constructal theory to ducts, rivers, turbulence, cracks, dendritic crystals and spatial economics, Int. J. Therm. Sci. 38 (1999) 653–663.

[4] A. Bejan, Thermodynamic optimization of geometry in engineering flow systems, Int. J. Exergy 1 (4) (2001) 269–277.

[5] A. Bejan, Dendritic constructal heat exchanger with small-scale crossflows and larger-scale counterflows, Int. J. Heat Mass Transfer 45 (2002) 4607–4620.

[6] Alexandre K. da Silva, Sylvie Lorente, Adrian Bejan, Constructal multi-scale tree-shaped heat exchangers, J. Appl. Phys. 96 (3) (2004) 1709–1718.

[7] A.K. da Silva, S. Lorente, A. Bejan, Constructal multi-scale structures for maximal heat transfer density, Energy 163 (2003) 39–49.

[8] Y.S. Muzychka, Constructal design of forced convection cooled microchannel heat sinks and heat exchangers, Int. J. Heat Mass Transfer 48 (2005) 3119–3127.

[9] J. Bonjour, L.A.O. Rocha, A. Bejan, F. Meunier, Dendritic fins optimization for a coaxial two-stream heat exchanger, Int. J. Heat Mass Transfer 47 (2003) 111–124.

[10] V.D. Zimparov, A.K. da Silva, A. Bejan, Thermodynamic optimization of tree-shaped flow geometries, Int. J. Heat Mass Transfer 49 (2006) 1619–1630.